



HAL
open science

The SCRIB Paralog LANO/LRRC1 Regulates Breast Cancer Stem Cell Fate through WNT/beta-Catenin Signaling

Leonor Lopez Almeida, Michael Sebbagh, Francois Bertucci, Pascal Finetti, Julien Wicinski, Sylvie Marchetto, Remy Castellano, Emmanuelle Josselin, Emmanuelle Charafe-Jauffret, Christophe Ginestier, et al.

► **To cite this version:**

Leonor Lopez Almeida, Michael Sebbagh, Francois Bertucci, Pascal Finetti, Julien Wicinski, et al.. The SCRIB Paralog LANO/LRRC1 Regulates Breast Cancer Stem Cell Fate through WNT/beta-Catenin Signaling. *Stem Cell Reports*, 2018, 11 (5), pp.1040-1050. 10.1016/j.stemcr.2018.09.008 . hal-02143631

HAL Id: hal-02143631

<https://amu.hal.science/hal-02143631>

Submitted on 3 Jun 2019

HAL is a multi-disciplinary open access archive for the deposit and dissemination of scientific research documents, whether they are published or not. The documents may come from teaching and research institutions in France or abroad, or from public or private research centers.

L'archive ouverte pluridisciplinaire **HAL**, est destinée au dépôt et à la diffusion de documents scientifiques de niveau recherche, publiés ou non, émanant des établissements d'enseignement et de recherche français ou étrangers, des laboratoires publics ou privés.



Distributed under a Creative Commons Attribution - NoDerivatives 4.0 International License



The *SCRIB* Paralog *LANO/LRRC1* Regulates Breast Cancer Stem Cell Fate through WNT/ β -Catenin Signaling

Leonor Lopez Almeida,^{1,5} Michael Sebbagh,^{1,5} François Bertucci,² Pascal Finetti,² Julien Wicinski,³ Sylvie Marchetto,¹ Rémy Castellano,⁴ Emmanuelle Josselin,⁴ Emmanuelle Charafe-Jauffret,³ Christophe Ginestier,³ Jean-Paul Borg,¹ and Marie-Josée Santoni^{1,*}

¹Centre de Recherche en Cancérologie de Marseille, CRCM, Aix Marseille University, Institut Paoli-Calmettes, CNRS, INSERM, 'Cell Polarity, Cell Signaling and Cancer'- Equipe Labellisée Ligue Contre le Cancer, Marseille, France

²Centre de Recherche en Cancérologie de Marseille, CRCM, Aix Marseille University, Institut Paoli-Calmettes, CNRS, INSERM, 'Predictive Oncology'- Equipe Labellisée Ligue Contre le Cancer, Marseille, France

³Centre de Recherche en Cancérologie de Marseille, CRCM, Aix Marseille University, Institut Paoli-Calmettes, CNRS, INSERM, 'Epithelial Stem Cells and Cancer', Marseille, France

⁴Centre de Recherche en Cancérologie de Marseille, CRCM, Aix Marseille University, Institut Paoli-Calmettes, CNRS, INSERM, TrGET Pre-clinical Assay Platform, Marseille, France

⁵Co-first author

*Correspondence: marie-josee.santoni@inserm.fr

<https://doi.org/10.1016/j.stemcr.2018.09.008>

SUMMARY

Tumor initiation, progression, and therapeutic resistance have been proposed to originate from a subset of tumor cells, cancer stem cells (CSCs). However, the current understanding of the mechanisms involved in their self-renewal and tumor initiation capacity remains limited. Here, we report that expression of *LANO/LRRC1*, the vertebrate paralog of *SCRIB* tumor suppressor, is associated with a stem cell signature in normal and tumoral mammary epithelia. Through *in vitro* and *in vivo* experiments including a *Lano/Lrrc1* knockout mouse model, we demonstrate its involvement in the regulation of breast CSC (bCSC) fate. Mechanistically, we demonstrate that *Lano/LRRC1*-depleted cells secrete increased levels of WNT ligands, which act in a paracrine manner to positively deregulate the WNT/ β -catenin pathway in bCSCs. In addition to describing the first function of *LANO/LRRC1*, our results suggest that its expression level could be used as a biomarker to stratify breast cancer patients who could benefit from WNT/ β -catenin signaling inhibitors.

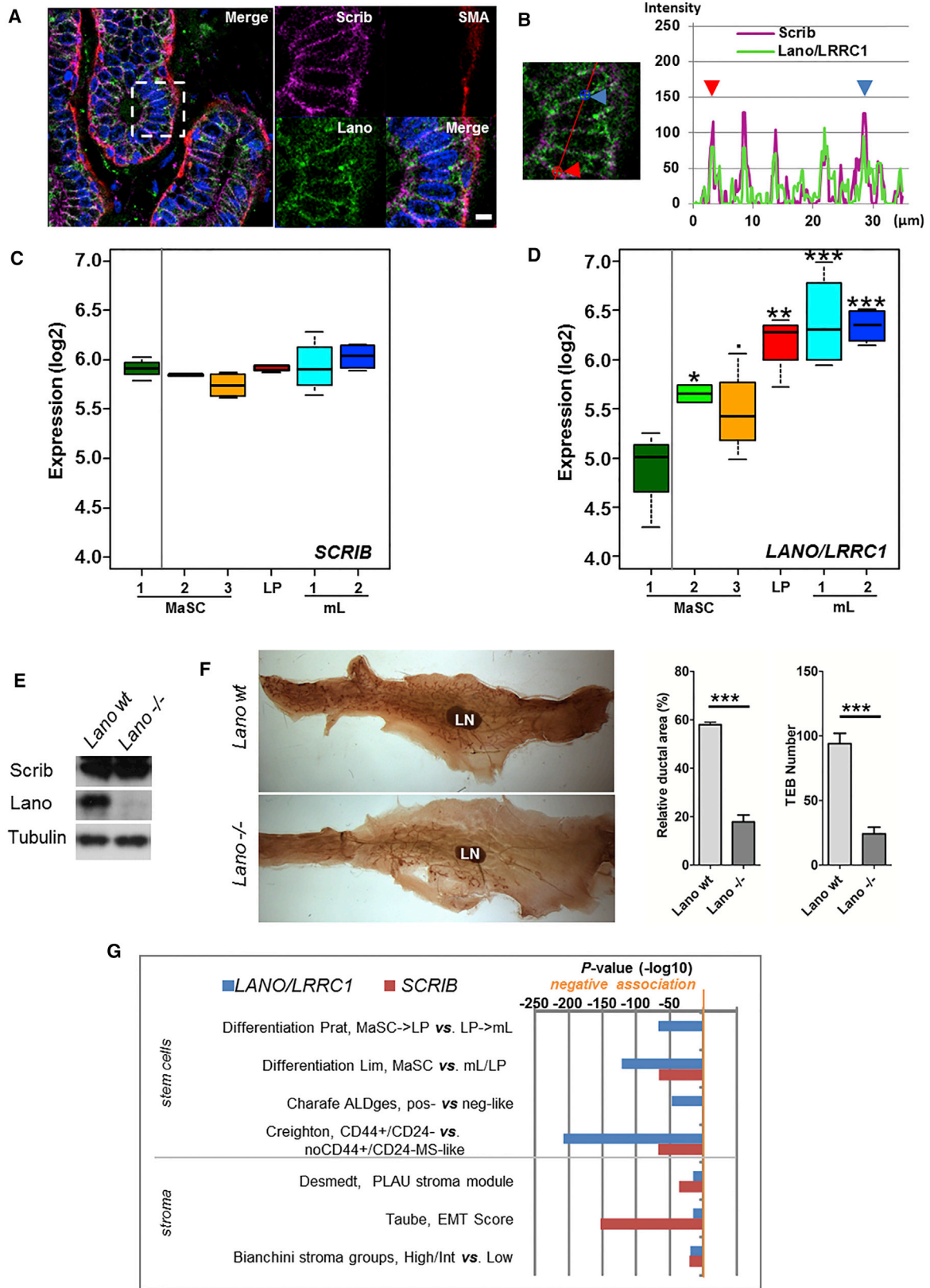
INTRODUCTION

Homeostasis of most tissues and organs results from constant regeneration and remodeling due to the function of adult stem cells, which are characterized by unlimited division capacity and the ability to give rise to all progenies of the differentiated cells required to form a functional tissue. Unsurprisingly, alterations of stem cell biology are associated with many human physiopathological disorders including cancer. Indeed, tumor heterogeneity stems, in part, from the presence of cancer stem cells (CSCs), a cellular population endowed with self-renewal properties able to initiate tumors (Visvader and Lindeman, 2012). In breast cancers, markers such as CD44 and aldehyde dehydrogenase (ALDH) allow the identification and purification of CSCs, the abundance of which correlates with tumor progression and metastatic spreading (Ginestier et al., 2007; Pece et al., 2010). Although the current understanding of the mechanisms of CSC emergence remains sparse, there is a consensus on the involvement of cell polarity alterations, notably due to the role of asymmetrical cell division in stem cell pool maintenance (Visvader and Lindeman, 2012). In addition, stem cells and CSC self-renewal have been linked to alterations of NOTCH, Hedgehog, Hippo (Yu et al., 2015), and WNT

(Nusse and Clevers, 2017) signaling, some of which have been causally linked to dysfunctional cell polarity. This is notably the case for Scrib, a LAP (LRR and PDZ) family member, which regulates planar cell polarity through Hippo and β -catenin independent WNT signaling (Sebbagh and Borg, 2014). *SCRIB* function has been extensively studied in mammary gland development (Godde et al., 2014) and cancer progression using *Scrib*-deficient (Zhan et al., 2008) or overexpressing (Feigin et al., 2014) mouse models. In breast cells, we and others have shown that loss of *SCRIB* expression impairs directional cell migration (Dow et al., 2007; Nola et al., 2008) and apico-basal cell polarity (Navarro et al., 2005) through the initiation of an EMT-like (epithelial-mesenchymal transition) process concomitantly with the acquisition of CSC properties (Cordenonsi et al., 2011).

We have previously cloned and characterized a mammalian *SCRIB* paralog, *LANO/LRRC1*, hereafter referred to as *Lano*, which encodes a protein sharing 60% amino acid identity with *SCRIB*, despite the lack of a PDZ domain (Saito et al., 2001; Santoni et al., 2002). Given the importance of *SCRIB* in mammary gland development (Godde et al., 2014) and in tumorigenesis (Cordenonsi et al., 2011; Feigin et al., 2014; Zhan et al., 2008), we decided to evaluate the contribution of *LANO* in these processes.





(legend on next page)



RESULTS

LANO and *SCRIB* Exhibit Different Expression Patterns in Mammary Epithelial Cell Hierarchy

To examine the potential role of *LANO* in normal human mammary gland, we first compared its expression pattern with that of *SCRIB* by immunofluorescence. *SCRIB* is mostly expressed in epithelial cells of the luminal layer (Godde et al., 2014) of the mammary gland and absent in the myoepithelial layer, as shown by smooth muscle antigen staining (Figure 1A). As reported, both proteins are mostly located at the basolateral membrane (Navarro et al., 2005; Saito et al., 2001) where they co-localize as illustrated by their intensity fluorescent profiles (Figure 1B) with a Pearson's correlation coefficient of 0.69 (± 0.03 , $n = 3$). Furthermore, the transcription profiles of *LANO* and *SCRIB* were extracted from a public RNA microarray dataset from the human mammary epithelial cell hierarchy (Morel et al., 2017). *SCRIB* mRNA levels are the same in all subsets of the human mammary epithelial cell hierarchy (Figure 1C). Interestingly, *LANO* transcript levels are unevenly distributed with low expression among the mammary stem cell (MaSC) subsets and increased levels along the luminal differentiation pathway, from luminal progenitors to mature luminal cells 1–2 (Figure 1D). Similar results (Figures S1A and S1B) were obtained from mouse counterpart datasets (Lim et al., 2010). To determine the consequences of loss of *Lano* function on mammary gland development, we generated a *Lano* knockout mouse strain (Figures S2B and S2C). Mice devoid of *Lano* are viable and fertile with a normal Mendelian distribution. Loss of *Lano* expression was confirmed by immunoblot on mammary gland lysates (Figure 1E). The kinetics of epithelial mammary ductal tree development was studied by Mayer's hemalum staining of 6-week-old mouse mammary glands. In *Lano* mutant mice, the growth of mammary ductal tree embedded in fat pad is significantly delayed (Figure 1F), which is correlated with a reduction in the number of terminal end buds (TEBs). The growth of mammary ductal tree recovers to normal levels at 12 weeks, when

mature mouse mammary glands of all genotypes appear normal (data not shown). While the involvement of *Scrib* in stem cell fate is established in various cellular contexts (Ono et al., 2015), in the mammary gland, stem cell fate seems not to be related to *Scrib* expression, nor is ductal tree development (Cordenonsi et al., 2011; Godde et al., 2014). Altogether, these data suggest that *Lano* contributes to MaSC fate and function in normal breast tissue as well as in early mouse mammary gland development.

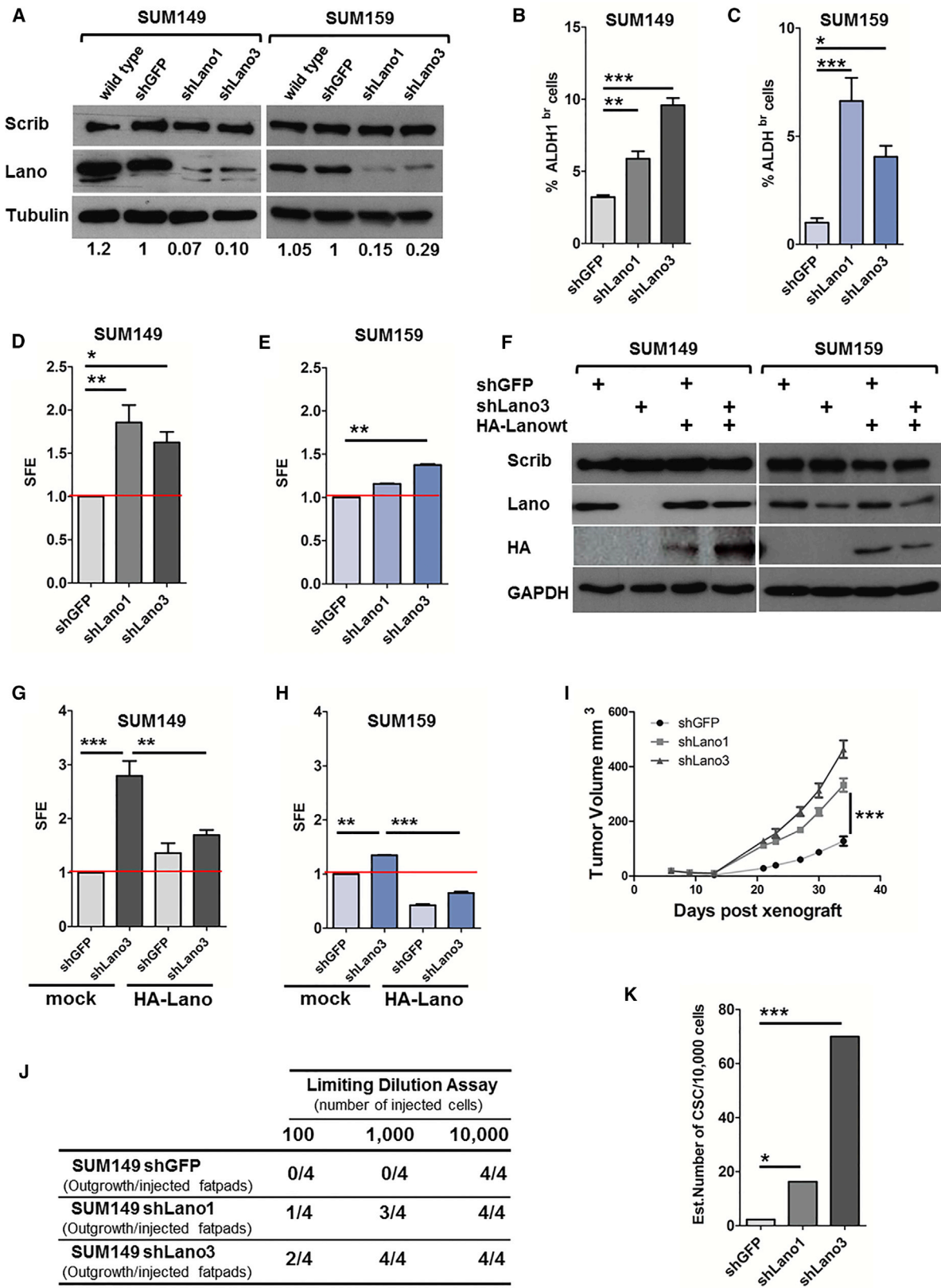
Low *LANO* Expression Is Associated with a CSC Signature in Human Breast Tumors

The differential expression of *LANO* in normal mammary gland cell populations led us to investigate a possible correlation between its mRNA levels and gene signatures in breast cancers. We carried out a univariate transcriptomic analysis using 9,057 patient tumor samples of all breast cancer subtypes gathered from 36 public datasets (Table S1). The results from these analyses (Figure 1G and Table S2) show that low *LANO* mRNA expression correlates with MaSC (Lim et al., 2010) and CSC signatures (Charafe-Jauffret et al., 2009; Creighton et al., 2009). In addition, *LANO* was also associated with a core EMT signature (Taube et al., 2010) which characterizes a process essential for the acquisition of stemness properties in normal and tumor cells (Mani et al., 2008). Similar analyses performed for *SCRIB* also show that low *SCRIB* transcript levels are associated with a CSC signature, as previously described (Cordenonsi et al., 2011), but to lesser extent than for *LANO*. Indeed, in contrast to *LANO*, the association of *SCRIB* with a CSC signature is limited to a subset of CSC markers, and no association was found with the Charafe-Jauffret and Prat signatures (Charafe-Jauffret et al., 2009; Prat et al., 2010). Conversely, the association of *SCRIB* with EMT signatures appears significantly stronger than that of *LANO* (Figure 1G and Table S2).

Thus, these results suggest that low *LANO* mRNA levels correlate with MaSC signatures in normal or pathological situations across all breast cancer subtypes.

Figure 1. *SCRIB* and *LANO* Expression in Human and Murine Mammary Gland

(A) *Scrib* and *Lano* immunofluorescence staining in normal human mammary gland sections with the indicated antibodies. Scale bar, 5 μ m. (B) Localization profiles of *Lano* and *Scrib* (right panel) along the red line are depicted in the left panel. (C–F) (C and D) Expression levels of *SCRIB* and *LANO/LRRC1* in human normal breast reported as a box plot. MaSC, mammary stem cell subsets; LP, luminal progenitors; mL, mature luminal cells. Statistical analysis was performed using one-way ANOVA with Tukey's post test. * $p < 0.05$, ** $p < 0.01$, *** $p < 0.001$. Pubescent 6-week-old mouse inguinal mammary glands of wild-type (wt) ($n = 2$) or *Lano* knockout mice ($n = 4$) were analyzed (E) by immunoblot for *Scrib* and *Lano* protein expression, with α -tubulin as loading control, and (F) by Mayer's hemalum whole-mount staining to visualize the epithelial tree. Lymph node (LN) is used as a marker (left panel). Quantifications of percentage of relative duct area (middle panel) and TEBs number (right panel) are shown. (G) Bar plots represent significance of univariate linear regression analysis of *LANO/LRRC1* (blue) and *SCRIB* (red) with stem cell and stroma signatures. Each bar score was defined as the log-transformed p value ($-\log_{10}$) and weighted by direction of association for analysis. Thus, at 5% risk, a score above 1.3 or under -1.3 was considered significant. ALDges, ALDH gene expression signature; MS-like, mammosphere-like; PLAU, plasminogen activator urokinase.



(legend on next page)



LANO Knockdown Leads to the Expansion of Breast CSCs

We then asked whether *LANO* expression, in addition to being a marker of cell differentiation, actively contributes to repress stemness properties of breast cancer cells. For this purpose, we used a short hairpin RNA (shRNA) approach to analyze the consequences of stable Lano depletion in two breast cancer cell lines, SUM149 and SUM159, which both contain a cell population subset (ALDH^{br}) with CSC-like features (Charafe-Jauffret et al., 2009). For each cell line, Lano-depleted cell populations were obtained using two different targeting sequences, shLano1 and shLano3. Knockdown efficiency was tested by immunoblot using parental cells or transfected by shRNA targeting the green fluorescent protein (shGFP) as controls (Figure 2A). In both cell lines, Lano expression was decreased to lower than 80% of wild-type levels while Scrib expression was unaffected, which demonstrates the specificity of the Lano-shRNAs. The use of a monoclonal antibody (811) binding a shared epitope of Lano and Scrib (Figure S2A) allowed us to compare their relative abundance and to exclude any compensation of *LANO* expression loss by *SCRIB*. The percentage of CSCs present in each SUM149 and SUM159 cell population was determined by measuring their ALDH enzymatic activity (Ginestier et al., 2007). SUM149 or SUM159 cell populations depleted for Lano contain two to five times more cells harboring ALDH activity than the corresponding shGFP control cells (Figures 2B and 2C). To functionally confirm the higher ALDH activity as the breast CSC (bCSC) population increases in Lano-depleted conditions we performed mammosphere assays, which indeed showed a significant fold increase of sphere-forming efficiency (SFE) in Lano-depleted cells compared with the shGFP control conditions in both cell lines (Figures 2D and 2E). To exclude a potential off-target effect, we carried out rescue experiments of mammosphere assays by re-expressing HA-tagged Lano, which confirmed the innocuity of ectopic expression of HA-Lano on Scrib expression levels (Figure 2F). As expected, the variations of SFE between Lano-depleted and control (shGFP) cells were abolished or

reverted by ectopic re-expression of HA-Lano (Figures 2G and 2H). Besides, to evaluate the impact on the tumorigenicity of cell populations depleted for Lano (or not), *in vivo* approaches were conducted through orthotopic xenografts of SUM149 cell populations in the fat pads of NOD/SCID/ γ c null immunodeficient mice (NSG) (Ginestier et al., 2007). Tumor growth kinetics showed that fat pads engrafted with 1×10^6 SUM149 cells devoid of Lano gave rise to tumors significantly faster than control conditions (Figure 2I). Through limiting dilution assays and analysis, the number of bCSCs was found to be lower in the control tumor cell population SUM149 shGFP, 1:4,326 (confidence interval [CI] 0.78–6.83) than in the Lano-depleted cell population SUM149 shLano1, 1:615 (CI 5.42–48.63, $p = 2.35 \times 10^{-2}$) and shLano3, 1:143 (CI 18.21–266.6, $p = 2.0 \times 10^{-4}$) (Figures 2J and 2K). These *in vivo* observations confirm our *in vitro* results and support a role of Lano in bCSC fate decision.

LANO Depletion Contributes to Metastatic Spreading

Because the bCSC population is described to be the seed of distant metastasis, we assessed whether *LANO* knockdown has an impact on cell motility and metastatic dissemination. First, we monitored the ability of shLano cells to disseminate to the lung and observed (Figure 3A) that shLano cells led to higher numbers of lung metastasis than shGFP-expressing cells. Besides, the higher metastatic capacity of Lano-deficient cells was correlated with their significantly higher velocity compared with control conditions, as measured by *in vitro* wound-healing assays on SUM149 and SUM159 (Figures 3B–3D), and confirmed by rescue experiments (Figures 3E and 3F). Altogether, these results demonstrate that *LANO* downregulation expands the bCSC compartment and contributes, at least in part, to metastatic dissemination.

LANO Regulates bCSC Fate through the Wnt/ β -Catenin Pathway

To define the molecular mechanism by which *LANO* affects bCSC fate determination, we first addressed

Figure 2. *LANO* Downregulation Increases Stemness Properties of bCSC Models *In Vitro* and *In Vivo*

(A) Immunoblot analysis of shGFP, shLano1, and shLano3 cell populations probed with the antibodies indicated. Quantification of Lano expression is indicated below.
(B and C) Percentage of ALDH^{br} cells for (B) SUM149 and (C) SUM159 ($n = 3$ for both).
(D and E) Sphere-forming efficiency (SFE) compared with the control of cell populations expressed as fold, for SUM149 (D; $n = 3$) and SUM159 (E; $n = 4$).
(F–H) SFE of SUM149 (G) and SUM159 (H) cells defined in (F) expressed as fold ($n = 3$).
(I) Kinetics of tumor growth of SUM149 cells of each population orthotopically xenografted in NSG mice.
(J and K) Table (J) showing the number of outgrowths generated as a function of the amount of injected cells (K). bCSC frequencies were calculated using an extreme limiting dilution analysis algorithm (shLano1 versus shGFP, $p = 0.0235$; shLano3 versus shGFP, $p = 0.0002$). Results are expressed as mean \pm SD, n for independent experiment, statistical significance using Kruskal-Wallis ANOVA with Dunnett's post test. * $p < 0.05$, ** $p < 0.01$, *** $p < 0.001$.



whether *LANO* has any effect on the stabilization of TAZ, a terminal effector of the Hippo pathway, as is the case for *SCRIB* (Cordenonsi et al., 2011). Since TAZ contributes to Hippo and WNT/ β -catenin (Yu et al., 2015) signaling, we measured the activation of both of them using firefly luciferase gene reporters under the control of TEAD or TCF/LEF response elements to monitor Hippo or WNT/ β -catenin transcriptional activities, respectively. Although Lano downregulation did not significantly affect TEAD transcriptional levels, it increased TCF/LEF activity 2-fold as compared with shGFP control conditions (Figure 4A). These results were confirmed by immunoblots in which TAZ and its paralog YAP expression levels appeared unaffected by loss of Lano expression, whereas active β -catenin levels were significantly increased (Figures 4B and 4C). Strikingly, whereas active β -catenin is normally resistant to degradation (Nusse and Clevers, 2017), its total expression levels did not seem to be affected. We hypothesized that this might be due to the restriction of WNT/ β -catenin upregulation to a subset of bCSCs affected by Lano knockdown. To test this possibility, we stained for active β -catenin sorted bCSC (ALDH^{hi}) and non-bCSC (ALDH^{neg}) cell populations depleted (or not) for Lano. It appeared that bCSCs from the Lano-depleted condition have significantly higher levels of active β -catenin than bCSCs from the shGFP control condition, while no variations were found in non-bCSCs (Figures 4D and 4E). Finally, rescue experiments were carried out in which ectopic expression of HA-tagged Lano restored active β -catenin levels (Figures 4F and 4G) as well as TCF/LEF transcriptional activity (Figure 4H) in shLano3 cell population to levels similar to that found in shGFP-transfected cells.

Overall these data suggest that *LANO* downregulation affects bCSC fate through a specific increase of WNT/ β -catenin activity.

Lano Represses WNT Ligand Secretion

Alterations of WNT/ β -catenin activity can be due to either a cell-autonomous process whereby cell signaling defects affect β -catenin degradation or nuclear shuttling (Nusse and Clevers, 2017), or non-cell-autonomous processes whereby defects are related to an imbalance between WNT ligand and its inhibitors, such as Dickkopf, in the cell environment (Niehrs, 2012; Nusse and Clevers, 2017). To define the underlying signaling between Lano and WNT/ β -catenin, we performed compartmentalized cultures of SUM149 shGFP cells with cells depleted of Lano separated by a porous membrane with 0.4 μ m pore size. After 48 hr, the shGFP cell population was harvested and subjected to immunoblot to monitor active and total β -catenin levels (Figures 4I and 4J). Similarly, mammosphere assays of shGFP cells were performed using condi-

tioned media originating from Lano-depleted cells (Figure 4K). These experiments revealed that SUM149 shGFP cells exhibit higher active β -catenin or mammosphere numbers when cultured with Lano-depleted cells or with their culture medium. These results suggest that Lano-deficient cells secrete soluble factors able to activate the WNT/ β -catenin signaling pathway. To assess whether this secreted factor might be a WNT ligand, we performed additional TCF/LEF luciferase assays of cells treated with IWP2, an inhibitor of Porcupine, an enzyme required for the final steps of WNT ligand maturation and its subsequent secretion. As shown in Figure 4L, IWP2 treatment reduced the WNT/ β -catenin activity of Lano-depleted cells to levels similar to those of control shGFP cell populations, showing the likely contribution of a WNT ligand. Since SUM149 and SUM159 cells have been described to secrete WNT3a ligand (El Helou et al., 2017), we quantified its abundance in the cell culture media by ELISA, and found it to be higher in both cell lines in Lano-depleted conditions (Figure 4M) than in the media of corresponding control cells. In addition, the impact of *LANO* depletion on WNT3a transcript levels was analyzed in both cell lines and did not reveal significant variation (Figure S1E). Finally, WNT3a transcription profiles extracted from public datasets from the human (Figure S1D) or mouse (Figure S1C) mammary epithelial hierarchy were also analyzed and appeared stable in all subsets, and therefore unrelated to *LANO* transcript levels. Altogether, these results strongly suggest that the WNT/ β -catenin activity of CSC observed in cells deficient for Lano is due, at least in part, to an increase in WNT3a secretion acting in a paracrine or autocrine manner.

DISCUSSION

In this study, we demonstrate that *LANO* expression regulates the stem cell fate of normal and tumor-derived mammary glands. Although a similar effect has been described for its paralog *SCRIB* (Cordenonsi et al., 2011; Godde et al., 2014), the mechanisms underlying this common feature are quite different. Downregulation of *SCRIB* or its delocalization triggers cell-autonomous signaling disorders mainly mediated through the Hippo pathway (Cordenonsi et al., 2011), whereas for *LANO* a cell-non-autonomous mechanism is involved through the secretion of WNT3a acting in a paracrine manner. In addition to these distinct molecular mechanisms, *SCRIB* and *LANO* differentially affect breast stem cell fates, as highlighted by the effect of their inactivation on mouse mammary gland development. Indeed, whereas *SCRIB* knockdown affects ductal luminal epithelium through altered polarity processes, notably stem cell asymmetric cell division, giving

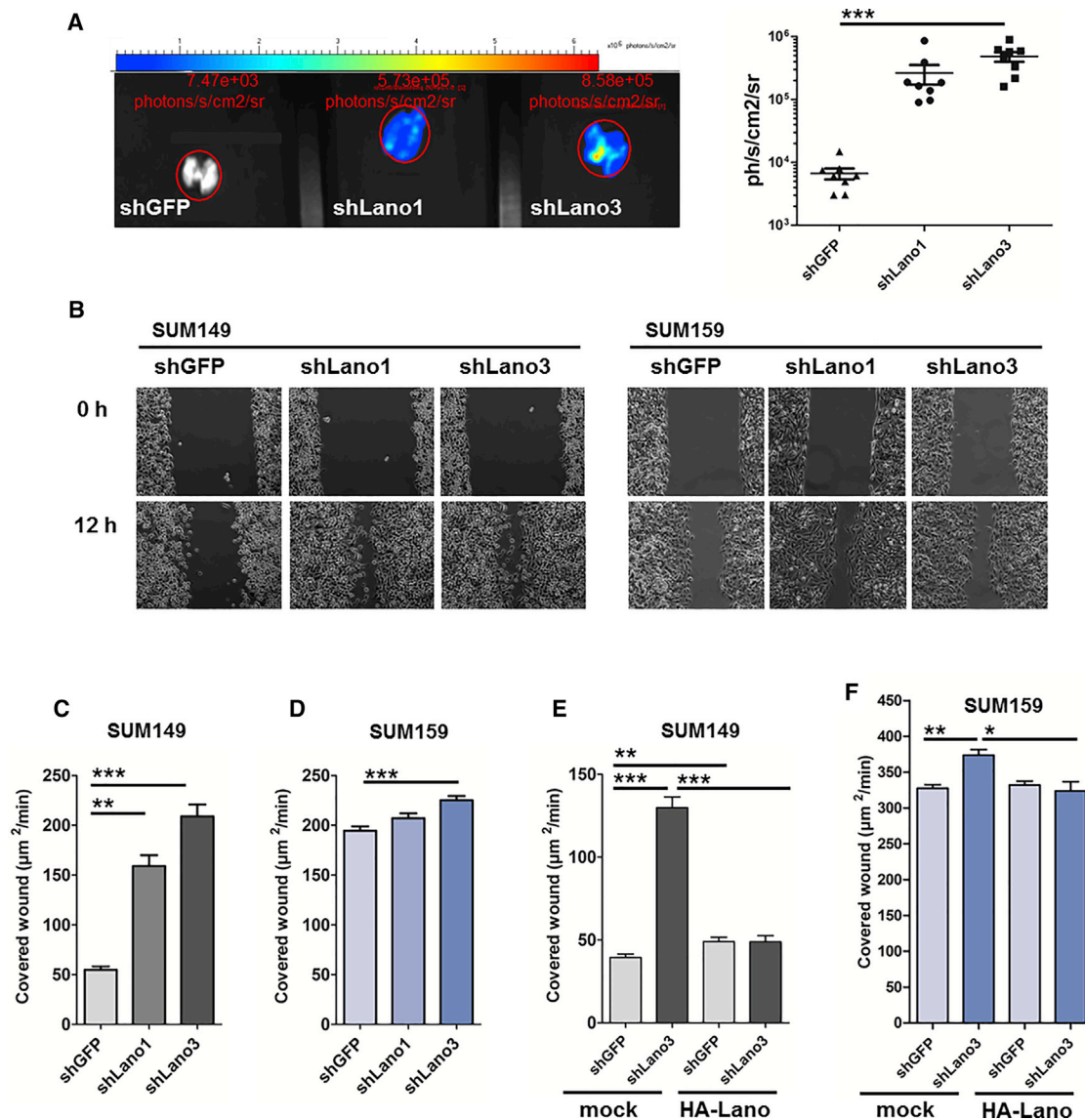


Figure 3. *LANO* Knockdown Contributes to Metastatic Spreading

(A) Representative microphotographs of metastatic lungs of xenografted mice described in Figure 2I, and chemoluminescence measurements by PhotonIMAGER in rainbow scale and related graph plotted.

(B) Representative images of wound-healing experiments for the shGFP, shLano1, and shLano3 SUM149 and SUM159 cell populations.

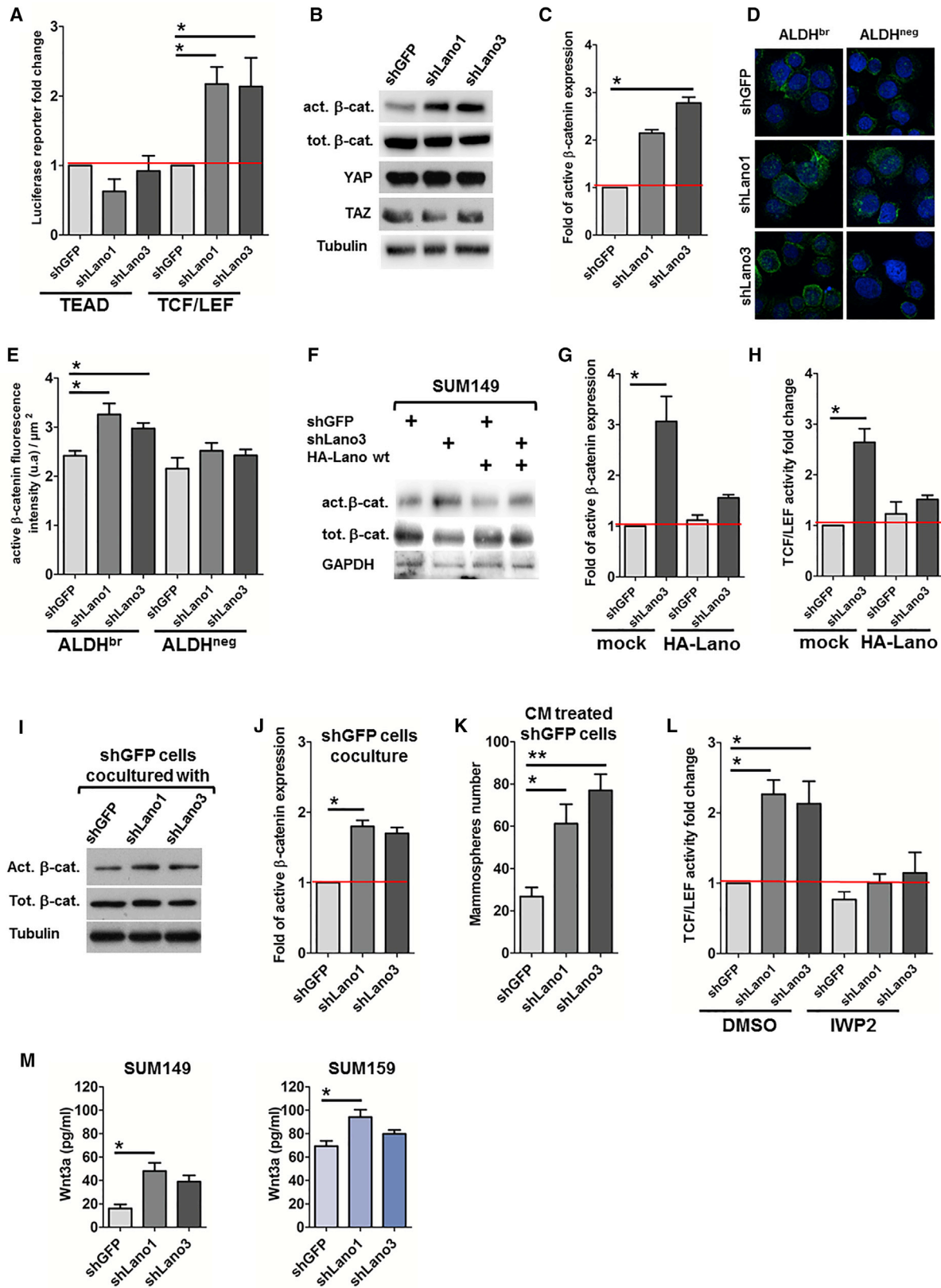
(C and D) Speed of wound closure represented in μm²/min for SUM149 (C) and SUM159 (D) (n = 4).

(E and F) Same as in (C) and (D) for cells expressing, or not, HA-tagged wild-type human Lano (n = 3).

Results are expressed as mean ± SD, n for independent experiment, statistical significance using Kruskal-Wallis ANOVA with Dunnett's post test. *p < 0.05, **p < 0.01, ***p < 0.001.

rise to a hyperbranched ductal tree (Godde et al., 2014), loss of Lano expression induces a delay in the development of the ductal epithelial tree, associated with hypo-branching and reduced numbers of TEBs, which may be due to an overproduction of MaSCs. Another difference between the two paralogs lies in their different roles in cancer cell migration, as Lano downregulation increases

velocity, in contrast to *SCRIB* loss (Dow et al., 2007; Nola et al., 2008). As the role of *SCRIB* in stem cell fate and self-renewal goes beyond the mammary epithelium (Ono et al., 2015), it will be interesting to study how Lano acts in other tissues, especially in the liver where its expression has been associated with hepatocellular carcinomas (Li et al., 2013). Although *SCRIB* and *LANO* are



(legend on next page)



phylogenetically and structurally related (Santoni et al., 2002), our results suggest that they have functionally diverged. Our work stresses the importance of defining how Lano impacts on WNT secretion in the extracellular medium. WNT transcriptional levels do not appear to be affected by Lano, which rather seems to be involved in WNT3a stabilization, maturation, or the repression of WNT ligand secretion, potentially through vesicular or exosomal pathways (Nusse and Clevers, 2017). Few Lano partners have been characterized. Among them we found Erbin (Saito et al., 2001), another LAP family member which has recently been involved in vesicular trafficking (Liu et al., 2018), and which might thus affect WNT secretion. Moreover, it will be worth assessing whether *Lano* expression could be used as a theranostic marker able to guide the administration of WNT signaling inhibitors. Thus, in breast tumors with low *Lano* expression, compounds targeting WNT signaling such as Porcupine inhibitors might be proposed as a therapeutic option, or drugs inhibiting WNT receptors (Frizzled) such as vantictumab, currently in phase I clinical trial (Fischer et al., 2017) for metastatic triple-negative breast cancers.

EXPERIMENTAL PROCEDURES

Gene Expression Data Analysis and Breast Cancer Samples

Data analysis of annotated clinical samples collected from 36 public datasets were performed using standard methods and are detailed in [Supplemental Experimental Procedures](#).

Statistical Analyses

Statistical analyses were performed using GraphPad Prism v5.03 (GraphPad Software), multiple variance analysis (ANOVA). The number of experiments and significant range are indicated in each legend.

ELISAs, Immunofluorescence, and Immunoblot Analysis

ELISAs, immunofluorescence, and immunoblot analysis were carried out according to Nola et al. (2008) and are detailed in [Supplemental Experimental Procedures](#).

Cell Culture

Cell culture was done according to El Helou et al. (2017) and is detailed in [Supplemental Experimental Procedures](#).

TCF/LEF Luciferase Report Assays

TCF/LEF luciferase report assays were carried out according to El Helou et al. (2017) and are detailed in [Supplemental Experimental Procedures](#).

TEAD Assays

TEAD assays were performed using the 8xGT1C promoter-luciferase reporter (#34615, Addgene).

Animal Models

All experiments were performed using standard methods, detailed in [Supplemental Experimental Procedures](#), in agreement with the French Guidelines for animal handling and approved by the local ethics committee APAFIS#10719-2017071709337799 v2.

SUPPLEMENTAL INFORMATION

Supplemental Information includes Supplemental Experimental Procedures, two figures, and two tables and can be found with this article online at <https://doi.org/10.1016/j.stemcr.2018.09.008>.

AUTHOR CONTRIBUTIONS

M.J.S., M.S., and L.L.A. designed, performed, and analyzed the experiments. R.C. and E.J. performed the xenograft experiments. F.C. and P.F. carried out *in silico* analysis. J.W., E.C.J., and C.G. conducted and analyzed ALDH and sphere activity. S.M. provided technical assistance. J.-P.B. provided advice as well as logistical and financial

Figure 4. *LANO* Represses Wnt Ligand Secretion

- (A) Fold induction of TEAD and TCF/LEF transcriptional activity by luciferase reporter assays (n = 6).
(B) Immunoblot analysis for the indicated antibodies.
(C) Fold induction of active β -catenin (act- β -cat) quantified by immunoblot (n = 3) related to shGFP.
(D) Representative microphotographs of SUM149 cell populations sorted for either ALDH^{br} or ALDH^{neg} status cytospinned and immunolabeled for active β -catenin antibody (green) and nucleus (blue).
(E) Quantification as fluorescent mean intensity of active β -catenin normalized by cell area (n = 2).
(F–H) (F) and (G) as in (B) and (C) for Lano rescued cell populations, and (H) their use in TCF/LEF transcriptional activity assay (n = 5).
(I and J) shGFP SUM149 cells were co-cultured with indicated cell population growing in Transwell insert prior immunoblot for active β -catenin analysis (I) and quantified as fold related to shGFP (J) (n = 3).
(K) Overnight cultured shGFP SUM149 cells were treated with the indicated conditioned medium (CM) prior to mammosphere formation assay (n = 3).
(L) TCF/LEF transcriptional assay, same as in (A) for cells treated for 15 hr with DMSO (vehicle) or 20 μ M IWP2 prior analysis (n = 4).
(M) Amount of WNT3a in culture medium measured by ELISA (n = 5).
Results are expressed as mean \pm SD, n for independent experiment, statistical significance using Kruskal-Wallis ANOVA with Dunnett's post test. *p < 0.05, **p < 0.01.



support. M.J.S. conceived and initiated the study and wrote the manuscript.

ACKNOWLEDGMENTS

We thank Institut Clinique de la Souris (Illkirch) for the Lano cKO mouse model; Géraldine Guasch-Grangeon, Gisèle Alcaraz, and Valérie Depraetere Ferrier for helpful discussions and manuscript proofreading; Stéphane Audebert for anti-Lano monoclonal antibodies production; Stefano Piccolo for the 8xGTIC reporter construct; Audrey Restouin, Armelle Goubard, Emilie Agavnian-Couquiaud, and Marie-Laure Thibult for excellent technical assistance; and Jean-Christophe Orsoni and Arnaud Capel for animal care. L.L.A. was a recipient of a PhD fellowship from “La Ligue Nationale Contre le Cancer.” This work was supported by Excellence Initiative of Aix-Marseille University – A*Midex, “Investissement d’avenir” (CapoStromEx); M.S. by CNRS-AMI Mécanobio (2016–2017); J.-P.B.’s lab by “La Ligue Nationale Contre le Cancer” (Label Ligue) and SIRIC (grant INCa-DGOS-Inserm 6038). J.-P.B. is a scholar of Institut Universitaire de France.

Received: December 14, 2017

Revised: September 18, 2018

Accepted: September 19, 2018

Published: October 18, 2018

REFERENCES

- Charafe-Jauffret, E., Ginestier, C., Iovino, F., Wicinski, J., Cervera, N., Finetti, P., Hur, M.H., Diebel, M.E., Monville, F., Dutcher, J., et al. (2009). Breast cancer cell lines contain functional cancer stem cells with metastatic capacity and a distinct molecular signature. *Cancer Res.* *69*, 1302–1313.
- Cordenonsi, M., Zanconato, F., Azzolin, L., Forcato, M., Rosato, A., Frasson, C., Inui, M., Montagner, M., Parenti, A.R., Poletti, A., et al. (2011). The Hippo transducer TAZ confers cancer stem cell-related traits on breast cancer cells. *Cell* *147*, 759–772.
- Creighton, C.J., Li, X., Landis, M., Dixon, J.M., Neumeister, V.M., Sjolund, A., Rimm, D.L., Wong, H., Rodriguez, A., Herschkowitz, J.I., et al. (2009). Residual breast cancers after conventional therapy display mesenchymal as well as tumor-initiating features. *Proc. Natl. Acad. Sci. U S A* *106*, 13820–13825.
- Dow, L.E., Kauffman, J.S., Caddy, J., Zarbalis, K., Peterson, A.S., Jane, S.M., Russell, S.M., and Humbert, P.O. (2007). The tumour-suppressor Scribble dictates cell polarity during directed epithelial migration: regulation of Rho GTPase recruitment to the leading edge. *Oncogene* *26*, 2272–2282.
- El Helou, R., Pinna, G., Cabaud, O., Wicinski, J., Bhajun, R., Guyon, L., Rioualen, C., Finetti, P., Gros, A., Mari, B., et al. (2017). miR-600 acts as a bimodal switch that regulates breast cancer stem cell fate through WNT signaling. *Cell Rep.* *18*, 2256–2268.
- Feigin, M.E., Akshinthala, S.D., Araki, K., Rosenberg, A.Z., Muthuswamy, L.B., Martin, B., Lehmann, B.D., Berman, H.K., Pietsch, J.A., Cardiff, R.D., et al. (2014). Mislocalization of the cell polarity protein scribble promotes mammary tumorigenesis and is associated with basal breast cancer. *Cancer Res.* *74*, 3180–3194.
- Fischer, M.M., Cancilla, B., Yeung, V.P., Cattaruzza, F., Chartier, C., Murriel, C.L., Cain, J., Tam, R., Cheng, C.Y., Evans, J.W., et al. (2017). WNT antagonists exhibit unique combinatorial antitumor activity with taxanes by potentiating mitotic cell death. *Sci. Adv.* *3*, e1700090.
- Ginestier, C., Hur, M.H., Charafe-Jauffret, E., Monville, F., Dutcher, J., Brown, M., Jacquemier, J., Viens, P., Kleer, C.G., Liu, S., et al. (2007). ALDH1 is a marker of normal and malignant human mammary stem cells and a predictor of poor clinical outcome. *Cell Stem Cell* *1*, 555–567.
- Godde, N.J., Sheridan, J.M., Smith, L.K., Pearson, H.B., Britt, K.L., Galea, R.C., Yates, L.L., Visvader, J.E., and Humbert, P.O. (2014). Scribble modulates the MAPK/Fra1 pathway to disrupt luminal and ductal integrity and suppress tumour formation in the mammary gland. *PLoS Genet.* *10*, e1004323.
- Li, Y., Zhou, B., Dai, J., Liu, R., and Han, Z.G. (2013). Aberrant up-regulation of LRRC1 contributes to human hepatocellular carcinoma. *Mol. Biol. Rep.* *40*, 4543–4551.
- Lim, E., Wu, D., Pal, B., Bouras, T., Asselin-Labat, M.L., Vaillant, F., Yagita, H., Lindeman, G.J., Smyth, G.K., and Visvader, J.E. (2010). Transcriptome analyses of mouse and human mammary cell subpopulations reveal multiple conserved genes and pathways. *Breast Cancer Res.* *12*, R21.
- Liu, H., Wang, S., Hang, W., Gao, J., Zhang, W., Cheng, Z., Yang, C., He, J., Zhou, J., Chen, J., et al. (2018). LET-413/Erbin acts as a RAB-5 effector to promote RAB-10 activation during endocytic recycling. *J. Cell Biol.* *217*, 299–314.
- Mani, S.A., Guo, W., Liao, M.J., Eaton, E.N., Ayyanan, A., Zhou, A.Y., Brooks, M., Reinhard, F., Zhang, C.C., Shipitsin, M., et al. (2008). The epithelial-mesenchymal transition generates cells with properties of stem cells. *Cell* *133*, 704–715.
- Morel, A.P., Ginestier, C., Pommier, R.M., Cabaud, O., Ruiz, E., Wicinski, J., Devouassoux-Shisheboran, M., Combaret, V., Finetti, P., Chassot, C., et al. (2017). A stemness-related ZEB1-MSRB3 axis governs cellular pliancy and breast cancer genome stability. *Nat. Med.* *23*, 568–578.
- Navarro, C., Nola, S., Audebert, S., Santoni, M.J., Arsanto, J.P., Ginestier, C., Marchetto, S., Jacquemier, J., Isnardon, D., Le Bivic, A., et al. (2005). Junctional recruitment of mammalian Scribble relies on E-cadherin engagement. *Oncogene* *24*, 4330–4339.
- Niehrs, C. (2012). The complex world of WNT receptor signalling. *Nat. Rev. Mol. Cell Biol.* *13*, 767–779.
- Nola, S., Sebbagh, M., Marchetto, S., Osmani, N., Nourry, C., Audebert, S., Navarro, C., Rachel, R., Montcouquiol, M., Sans, N., et al. (2008). Scrib regulates PAK activity during the cell migration process. *Hum. Mol. Genet.* *17*, 3552–3565.
- Nusse, R., and Clevers, H. (2017). Wnt/beta-catenin signaling, disease, and emerging therapeutic modalities. *Cell* *169*, 985–999.
- Ono, Y., Urata, Y., Goto, S., Nakagawa, S., Humbert, P.O., Li, T.S., and Zammit, P.S. (2015). Muscle stem cell fate is controlled by the cell-polarity protein Scrib. *Cell Rep.* *10*, 1135–1148.
- Pece, S., Tosoni, D., Confalonieri, S., Mazzarol, G., Vecchi, M., Ronzoni, S., Bernard, L., Viale, G., Pelicci, P.G., and Di Fiore, P.P. (2010). Biological and molecular heterogeneity of breast cancers correlates with their cancer stem cell content. *Cell* *140*, 62–73.



- Prat, A., Parker, J.S., Karginova, O., Fan, C., Livasy, C., Herschkowitz, J.I., He, X., and Perou, C.M. (2010). Phenotypic and molecular characterization of the claudin-low intrinsic subtype of breast cancer. *Breast Cancer Res.* *12*, R68.
- Saito, H., Santoni, M.J., Arsanto, J.P., Jaulin-Bastard, F., Le Bivic, A., Marchetto, S., Audebert, S., Isnardon, D., Adelaide, J., Birnbaum, D., et al. (2001). Lano, a novel LAP protein directly connected to MAGUK proteins in epithelial cells. *J. Biol. Chem.* *276*, 32051–32055.
- Santoni, M.J., Pontarotti, P., Birnbaum, D., and Borg, J.P. (2002). The LAP family: a phylogenetic point of view. *Trends Genet.* *18*, 494–497.
- Sebbagh, M., and Borg, J.P. (2014). Insight into planar cell polarity. *Exp. Cell Res.* *328*, 284–295.
- Taube, J.H., Herschkowitz, J.I., Komurov, K., Zhou, A.Y., Gupta, S., Yang, J., Hartwell, K., Onder, T.T., Gupta, P.B., Evans, K.W., et al. (2010). Core epithelial-to-mesenchymal transition interactome gene-expression signature is associated with claudin-low and metaplastic breast cancer subtypes. *Proc. Natl. Acad. Sci. U S A* *107*, 15449–15454.
- Visvader, J.E., and Lindeman, G.J. (2012). Cancer stem cells: current status and evolving complexities. *Cell Stem Cell* *10*, 717–728.
- Yu, F.X., Zhao, B., and Guan, K.L. (2015). Hippo pathway in organ size control, tissue homeostasis, and cancer. *Cell* *163*, 811–828.
- Zhan, L., Rosenberg, A., Bergami, K.C., Yu, M., Xuan, Z., Jaffe, A.B., Allred, C., and Muthuswamy, S.K. (2008). Deregulation of scribble promotes mammary tumorigenesis and reveals a role for cell polarity in carcinoma. *Cell* *135*, 865–878.

Stem Cell Reports, Volume 11

Supplemental Information

The *SCRIB* Paralog *LANO/LRRC1* Regulates Breast Cancer Stem Cell Fate through WNT/ β -Catenin Signaling

Leonor Lopez Almeida, Michael Sebbagh, François Bertucci, Pascal Finetti, Julien Wicinski, Sylvie Marchetto, Rémy Castellano, Emmanuelle Josselin, Emmanuelle Charafe-Jauffret, Christophe Ginestier, Jean-Paul Borg, and Marie-Josée Santoni

The *SCRIB* Paralog *LANO/LRRC1* Regulates Breast Cancer Stem Cell Fate through WNT/ β -catenin Signaling

Leonor Lopez Almeida, Michael Sebbagh, François Bertucci, Pascal Finetti, Julien Wicinski, Sylvie Marchetto, Rémy Castellano, Emmanuelle Josselin, Emmanuelle Charafe-Jauffret, Christophe Ginestier, Jean-Paul Borg and Marie-Josée Santoni

SUPPLEMENTAL INFORMATION

Inventory of Supplemental Information

Supplemental Figures S1-S2 and Legends and Tables S1-S2

Figure S1 related to main Figure 1 and 4

Figure S2 related to main Figure 1

Tables S1-S2 related to Figure 1

Supplemental Experimental Procedures

Supplemental References

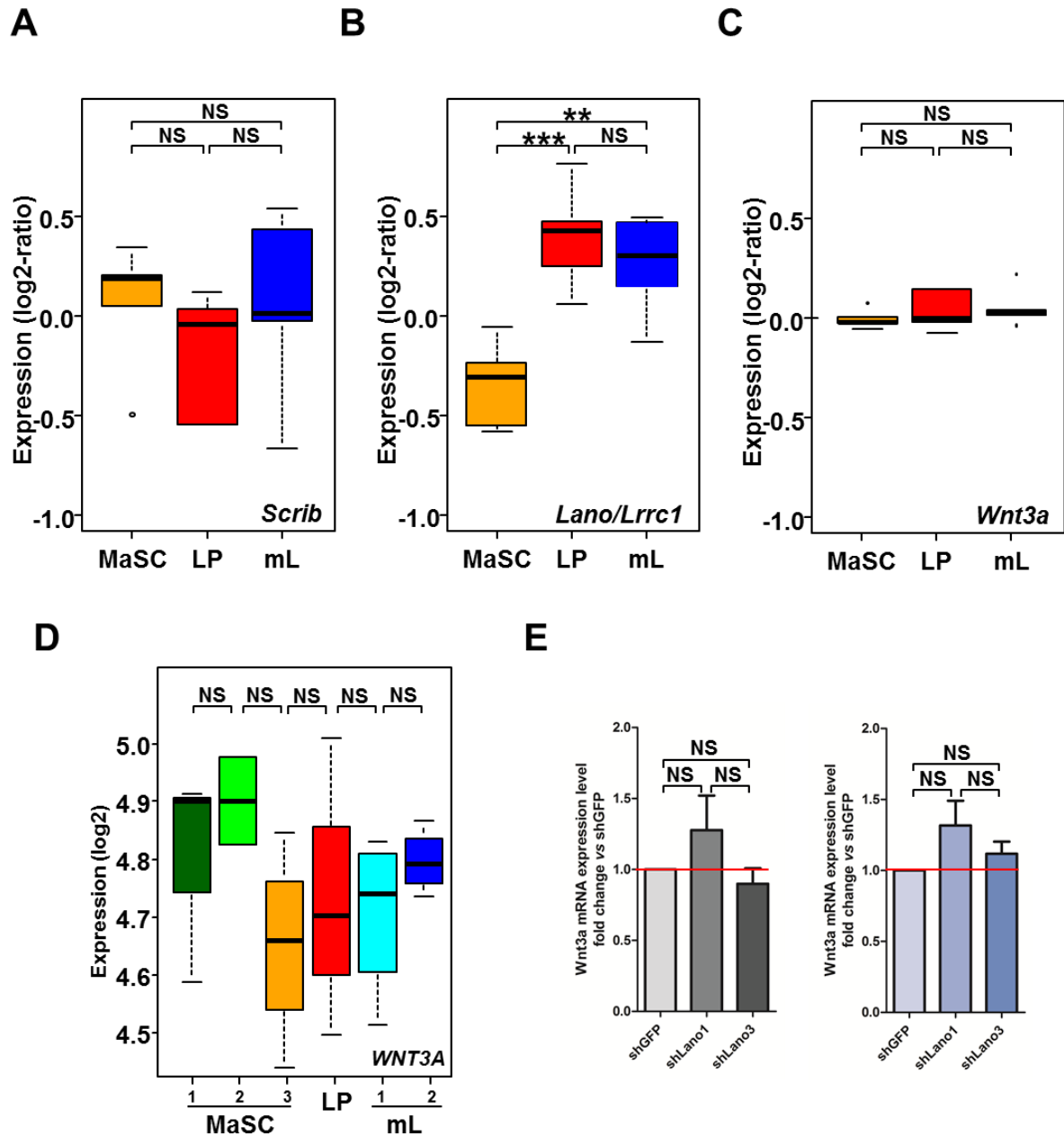


Figure S1: *LANO/LRRC1*, *SCRIB* and *WNT3A* Transcriptomic Expression.
Relative to main Figure 1 and 4.

(A) Expression levels of *SCRIB* and (B) *Lano/LRRC1*, (C) *WNT3A* in murine normal breast reported as a box-plot according to the three Lim's mammary epithelial cell hierarchy subsets. (D) Same than in (C) for human normal breast according to Morel et al, 2017. Statistical analysis was performed using one way ANOVA with Tukey post-test. NS (not significant), *P < 0.05; **P < 0.01; ***P < 0.001. (E) *WNT3A* transcript level expressed as fold changed relative to shGFP measured by Q-PCR in SUM149 (n=3) and SUM159 (n=3) cell populations. Results are expressed as mean ± SD, n for independent experiment, statistical significant using Kruskal-Wallis ANOVA with Dunnett's post-test, NS (not significant), *p < 0.05, **p < 0.01, ***p < 0.001.

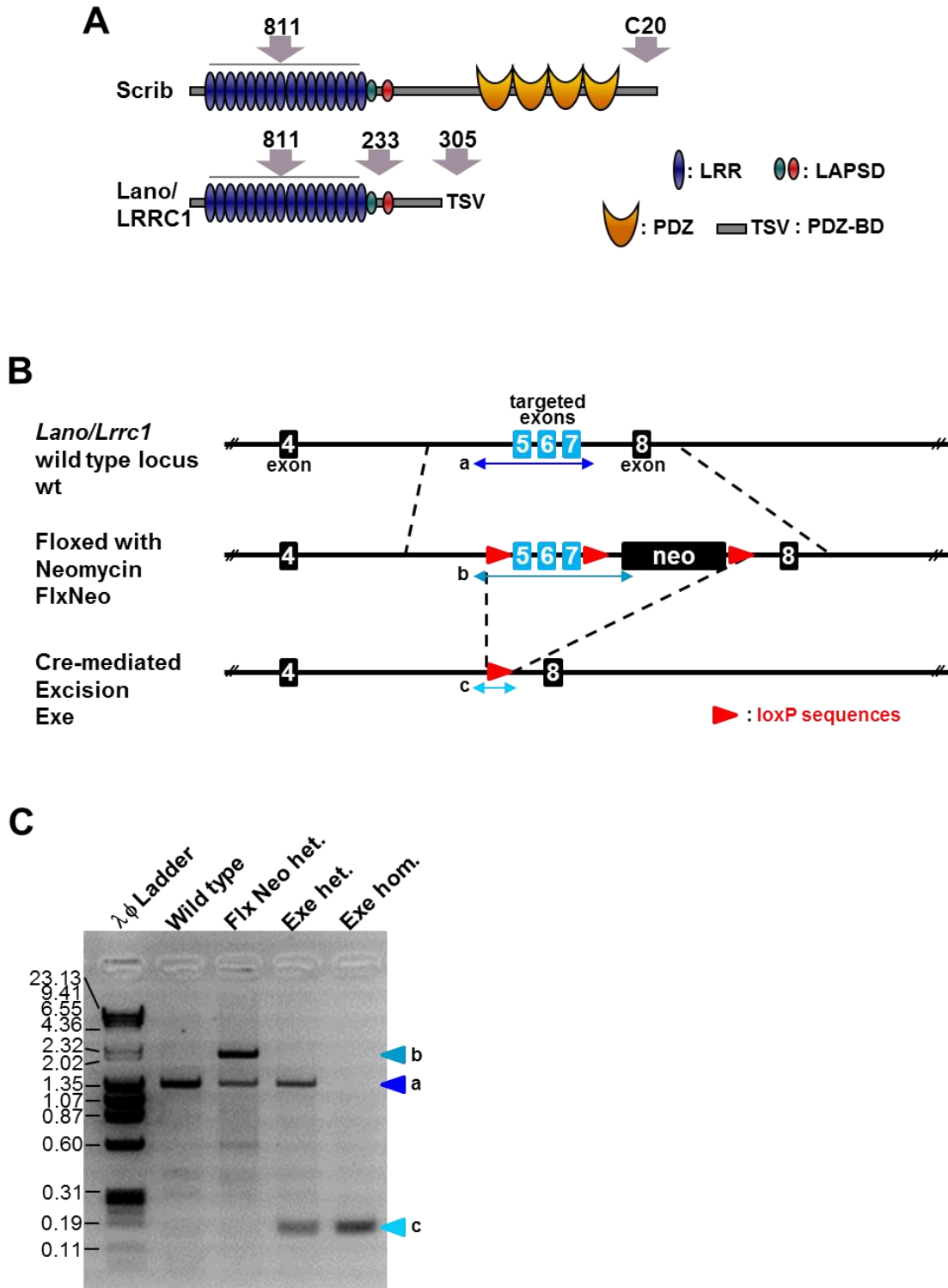


Figure S2: Structures of Lano/Lrrc1 protein and gene. Relative to main Figure 1.

(A) Scrib and Lano/LRRC1 general protein structure and localization of the antibodies epitopes used in this study. (B) Scheme for the generation of the *Lano/LRRC1* conditional knockout, Neo for Neomycin. (C) PCR profiles obtained from genomic DNA templates used to differentiate between mouse genotypes: wt (wild type), Flx-Neo-Het (unexcized heterozygous), Exe het (excized heterozygous), Exe hom (excized homozygous). On the left, Ladder scale in kb (mixture of Lambda-HindIII and Φ X174-HaeIII). On the right, fragment amplifications display on the scheme in (B).

Table S1.
List of data sets included in this study.
Relative to main Figure 1.

Reference	Source of data	N° of samples	Technological platform	N° of probe sets	N° of samples used
van de Vijver et al., NEJM 2002	http://microarray-pubs.stanford.edu/wound_NKI/	295	Agilent Hu25K	25K	254
van't Veer et al., Nature 2002	http://www.rii.com/publications/2002/vantveer.html	117	Agilent Hu25K	25K	117
Expression Project for Oncology (expO), 2005	GEO: GSE2109	348	Affymetrix U133 Plus 2.0	54K	348
Farmer Pet al., Oncogene 2005	GEO: GSE1561	49	Affymetrix U133A	22K	49
Minn AJ et al., Nature 2005	GEO: GSE2603	99	Affymetrix U133A	22K	99
Wang Y et al., Lancet 2005	GEO: GSE2034	286	Affymetrix U133A	22K	286
Hess KR et al., J Clin Oncol 2006	MDA133	133	Affymetrix U133A	22K	133
Ivshina et al., Cancer Res 2006	GEO: GSE4922, GSE1456	448	Affymetrix U133A+B	2x22K	448
Sotiriou C et al., J Natl Cancer Inst 2006	GEO: GSE2990	189	Affymetrix U133A	22K	80
Bonnefoi et al., Lancet Oncol 2007	GEO: GSE6861, GSE4779	161	Affymetrix X3P	61K	125
Desmedt C et al., Clin Cancer Res 2007	GEO: GSE7390	198	Affymetrix U133A	22K	154
Miller WR et al., Breast Cancer Res 2010	GEO: GSE5462	116	Affymetrix U133A	22K	116
Klein A et al., Int J Cancer 2007	GEO: GSE6596	26	Affymetrix U133A	22K	24
Hoeflich et al., Clin Cancer Res 2009	GEO: GSE12763	30	Affymetrix U133 Plus 2.0	54K	30
Marty et al., Breast Cancer Res 2008	GEO: GSE13787	23	Affymetrix U133 Plus 2.0	54K	23
Merritt WM et al., N Engl J Med 2008	Array Express: E-MTAB-158	130	Affymetrix U133AAofAv2	23K	130
Schmidt M et al., Cancer Res 2008	GEO: GSE11121	200	Affymetrix U133A	22K	200
Yu K et al., PLoS Genet 2008	GEO: GSE5364	196	Affymetrix U133A	22K	183
Bos P et al., Nature 2009	GEO: GSE12276	204	Affymetrix U133 Plus 2.0	54K	204
Zhang Y et al., Breast Cancer Res Treat 2009	GEO: GSE12093	136	Affymetrix U133A	22K	136
Barry et al., J Clin Oncol 2010	GEO: GSE23593	50	Affymetrix U133 Plus 2.0	54K	50
Iwamoto T et al., J Natl Cancer Inst 2011	GEO: GSE22093, GSE22597	247	Affymetrix U133A	22K	100
Korde et al., Breast Cancer Res Treat 2010	GEO: GSE18728	61	Affymetrix U133 Plus 2.0	54K	61
Prat A et al., Breast Cancer Res 2010	GEO: GSE18229	337	Agilent Hu25K	25K	264
Silver et al., J Clin Oncol 2010	GEO: GSE18864	84	Affymetrix U133 Plus 2.0	54K	84
Tabchy A et al., Clin Cancer Res 2010	GEO: GSE20271	178	Affymetrix U133A	22K	178
Jonsson et al., BCR 2010	GEO: GSE22133	359	Swegene H_v2.1.1 55K	55K	346
Chen et al., Breast Cancer Res Treat 2010	GEO: GSE10780	185	Affymetrix U133 Plus 2.0	54K	42
Sabattier R et al., PLoS One 2011	GEO: GSE31448	353	Affymetrix U133 Plus 2.0	54K	352
Desmedt et al., J Clin Oncol 2011	GEO: GSE16446	120	Affymetrix U133 Plus 2.0	54K	120
Guedj et al., Oncogene 2011	Array Express: E-MTAB-365	537	Affymetrix U133 Plus 2.0	54K	452
Hatzis C et al., JAMA 2011	GEO: GSE25066	508	Affymetrix U133A	22K	508
Popovici V et al., Breast Cancer Res 2010	GEO: GSE20194	278	Affymetrix U133A	22K	91
TCGA, Nature 2012	TCGA Data Portal - BRCA-	1215	illumina, RNAseq V2	20K	1095
Ellis et al., Nature 2012	GEO: GSE29442, GSE35186	201	Agilent-0148504x44K	44K	201
Curtis et al., Nature 2012	EGA: EGAS00000000083	2136	illumina HT 12	49K	1974
TOTAL		10233			9057

Table S2.

Univariate linear regression analysis of *Lano/LRRC1* and *SCRIB* with stem cell and stroma signatures. Relative to main Figure 1.

		<i>SCRIB</i>			<i>Lano/LRRC1</i>		
		N	Odds ratio [CI95]	P-value	N	Odds ratio [CI95]	P-value
stem cells	Differentiation Prat, pL->mL vs. MaSC->pL	8539	0.97 [0.94-0.99]	4.81E-02	9039	1.31 [1.28-1.35]	3.73E-67
	Differentiation Lim, mL vs. MaSC	8539	1.20 [1.16-1.24]	5.04E-67	9039	1.55 [1.51-1.60]	3.61E-122
	pL vs. MaSC	8539	1.43 [1.38-1.48]		9039	1.29 [1.25-1.33]	
	Charafe ALDges, neg- vs pos-like	8539	0.96 [0.93-0.99]	1.60E-02	9039	1.35 [1.52-1.61]	1.66E-47
	Creighton, noCD44+/CD24- vs. CD44+/CD24- MS-like	8539	1.60 [1.53-1.67]	1.18E-68	9039	2.13 [2.05-2.21]	6.60E-209
stroma	Desmedt, PLAU stroma module	8403	0.88 [0.86-0.89]	4.03E-37	8903	0.93 [0.91-0.94]	1.53E-15
	Taube, EMT Score	8539	0.67 [0.65-0.69]	6.15E-154	9039	0.89 [0.87-0.91]	7.50E-16
	Bianchini stroma groups, High vs. Low	8537	0.82 [0.79-0.85]	1.40E-21	9037	0.84 [0.81-0.86]	4.58E-20
	Int vs. Low	8537	0.92 [0.89-0.95]		9037	0.93 [0.91-0.96]	

Supplemental Experimental Procedures

Gene expression data analysis, breast cancer samples

Data analysis of annotated clinical samples collected from 36 public data sets (Table S1) required pre-analytic processing. The first step was to normalize each data set separately: we used quantile normalization for the available processed data from non-Affymetrix-based sets (Agilent, SweGene and Illumina), and Robust Multichip Average (RMA) with the non-parametric quantile algorithm for the raw data from the Affymetrix-based data sets. Normalization was done in R using Bioconductor and associated packages. Then, hybridization probes were mapped across the different technological platforms represented. We used SOURCE (<http://smd.stanford.edu/cgi-bin/source/sourceSearch>) and EntrezGene (Homo sapiens gene information db, 09/12/2008, release, <ftp://ftp.ncbi.nlm.nih.gov/gene/>) to retrieve and update the non-Affymetrix gene chips annotations, and NetAffx Annotation files (www.affymetrix.com; release from 01/12/2008) to update the Affymetrix gene chips annotations. The probes were then mapped based on their EntrezGeneID. When multiple probes mapped to the same GeneID, we retained the one with the highest variance in a particular dataset. We log₂-transformed the available TCGA RNAseq data that were already normalized. We applied different multigene classifiers in each data set separately. The intrinsic molecular subtypes of tumors were defined using the PAM50 classifier (Parker et al., 2009) as previously described (Finetti et al., 2008). *LRRC1* and *SCRIB* expression level were extracted from each of the 36 normalized data sets. Before analysis, gene expression data were standardized within each data set using the PAM50 luminal A population as reference. This allowed to exclude biases due to laboratory-specific variations and to population heterogeneity and to make data comparable across all sets.

Association of both *LRRC1* and *SCRIB* expression with stem cells and stroma multigene classifiers was evaluated in univariate linear regression analysis using the glm function in R's statistical package. All statistical tests were two-sided at the 5% level of significance. Statistical analysis was done using the R software (version 2.15.2; <http://www.cran.r-project.org/>).

Immunofluorescence

Paraffin embedded human breast tissue sections were deparaffinized and rehydrated by Histolemon and alcohol baths respectively. Antigen retrieval was done in Sodium citrate 10mM pH6 at 97°C for 20min before incubation in blocking buffer 1 hour at 4°C. Tissues were labelled with Lano_233 antibody (Saito et al., 2001), Scrib (C20 Santa-Cruz Biotechnology) and anti- α SMA antibodies (A2547 Sigma) overnight at 4°C washed in PBS, and then incubated for 1h with donkey Alexa Fluor®-conjugated secondary antibodies and Hoechst 33342 (1 μ g mL⁻¹) for nuclear staining. Coverslips were then washed and mounted using ProlongGold® (Thermo-Fisher, France). Images were acquired using a Zeiss Axiovert 200 MOT microscope coupled to a LSM880 confocal module operated by Zeiss Zen 2015 software (Carl Zeiss MicroImaging, Inc., Germany) using either a 40x (PlanApochromat, NA 1.3) or a 63X oil-immersion objective (PlanApochromat, NA 1.4). Staining of cytospined cells were fixed by paraformaldehyde 4% for 10 min, permeabilized by triton 0.1% 5 min and stained for active β -catenin (#19807, Cell signaling technology) as above. To quantify β -catenin, Z-stack of five 16 bits 1024x1024 images of each condition was processed using Image J. Mean intensities normalized by cell area from at least 100 cells corresponding to five different fields were measured after Z-projection, smooth filtered.

Immunoblot analysis

Cells were lysated in ice-cold lysis buffer containing Hepes 50mM pH7.5, EGTA 1mM, NaCl 150mM, MgCL2 1.2mM, Glycerol 10%, Triton X-100 1% and Proteinase Inhibitor Cocktail and Phosphatase Inhibitor Cocktail. Typically, 25 μ g cell lysates were migrated in 7.5% SDS-PAGE (Sodium Dodecyl Sulfate-PolyAcrylamide Gel Electrophoresis) and transferred onto AmershamTM ProtranTM Supported 0.45 μ m NC (GE Healthcare Bio-Sciences, Piscataway, NJ, USA).

The primary antibodies used were anti-Lano/Scrib 8.8.1 (home-made mouse monoclonal antibody), anti- β -catenin (Cell Signaling L87A12), anti-active β -catenin/Non-phospho β -Catenin (Ser33/37/Thr41) (Cell signaling D13A1), anti-HA mAb (Covance). The control loading used were anti- α -Tubulin from (Abcam ab11317) or anti-GAPDH (Abcam (ab8245)).

Wnt3a ELISA test

Supernatants of our cells of interest were collected after a 4 days culture, concentrated with centrifuge filter 10,000 MW cut off (#P33361, Life Technologies) and then submitted to an ELISA test done with the Wnt3a ELISA kit (#E34-022639, Neo Biotech) according to the manufacturer's recommendations.

Cell culture conditions

SUM149 (basal) and SUM159 (mesenchymal) human breast cancer cell lines were cultured in F12-Hams (Mix (1X) Glutamax, (Gibco™) supplemented with 5% heat inactivated fetal bovine serum, 2µg/ml human insulin, 0,5 mg of 1µg/ml hydrocortisone and 1X NEAA, Non-Essential Amino Acids (11140-050 Gibco™).

Cell transfection

Typically, 10⁶ SUM149 or SUM159 cells were nucleofected with 2µg of the plasmid of interest using AMAXA kit solution V and program V-001 as recommended by the manufacturer (Lonza). The Lano/LRRC1 shRNA pSUPER constructs contained the following interfering sequences Lano1: GCTTGGACTTAGTGATAATGA or Lano3: GCACTGGAGAAGCTTGGTAAAT. The shGFP pSUPER construct used as a control was described in (Sebbagh et al., 2009). Rescue HA-Tagged Lano/LRRC1 construct was described in (Saito et al 2001) and submitted to site-directed mutagenesis to become shLano3 resistant (Invitrogen).

Culture with conditioned medium and Transwell Co-culture

Control shGFP SUM149 cells were grown at the bottom of 6-wells plates and culture either with conditioned media (CM) produced either by shGFP, shLano1 or shLano3 SUM149 cells or co-culture with these cells separated by 0.4µm polycarbonate membrane (Transwell, Costar, 3412). After 48 hours, shGFP cells growing at the bottom of well plate were harvest for indicated assay.

ALDH activity and Mammosphere forming assay

ALDEFLUOR assay (Stem Cell Technologies) used to measure the ALDH activity and the functional mammosphere forming assay were described (El Helou et al., 2017).

Wound healing assay

SUM149 cells were seeded into culture inserts (Ibidi, Martinsried, Germany) in 12-wells plates at 2000 cells/insert. After 24h inserts were removed, cells cultured in media supplemented with mytomicin C (1µg/ml) and monitored every 10 minutes for 24 hours by Time lapse video microscope (Axiovert 200, Zeiss). Images were analyzed with Metamorph software.

TEAD and TCF/LEF luciferase assay

SUM149 cells were nucleofected with AMAXA kit V and the V-001 program. In brief for 2X 10⁶ of SUM149 cells were treated with a mixture of 2µg 8xGTIC promoter-luciferase reporter (#34615, Addgene) (or TCF/LEF luciferase reporter) with 0.2 µg pRL-TK-Renilla. 24 hours later, cells were lysed and luciferase activity was measured using a dual-luciferase reporter assay system (#E1960; Promega) according to the manufacturer's instructions. Luciferase activity was measured by a GLOMAX 20/20 luminometer (Promega). Transfection efficiency was normalized to thymidine kinase promoter-driven Renilla luciferase (pRL-TK) activity as the internal control.

RNA extraction and quantitative RT and Q-PCR

RNA extractions from cells and mouse tissues were performed using the RNeasy Mini kit (#74104), including DNase sample treatment, according to the supplier's recommendations (Qiagen, France). Random-primer reverse transcription was performed using Superscript II reverse transcriptase (Thermo Fisher, France). Q-PCR was performed using SYBR green PCR master mix, and thermal cycling was conducted in in the thermocycler CFX96 Real time System (Bio Rad). WNT3a Q-PCR was performed using Fw: CCGTGCTGGACAAAGCTACC, Rv: TGAGCGTGCTCACTGCAAAGG and normalized to the expression of the housekeeping gene GAPDH (Fw: CAACGGATTTGGCCGTATTGG; Rv: TGAAGGGGTCATTGATGGCG) and/or beta-glucuronidase (Fw: CGCCCTGCCTATCTGTATTTC ; Rv: TCCCCACAGGGAGTGTGTAG).

Animal models

The *Lano/LRRC1* cKO was generated by the Mouse Clinical Institute from the vector design to the characterization of the chimera's mutation transmission (MCI Illkirch, France). To obtain *Lano/LRRC1* conditional knock out (*Lano* cKO) mice, original *Lano/LRRC1* exons 5 to 7 were replaced by these exons followed by a neomycine-resistance cassette both flanked by loxP sites using homologous recombination. To obtain a *Lano* null (*Lano*^{-/-}) mouse strain, *Lano* cKO mice were mated with transgenic mice expressing a CMV driven Cre recombinase which activates ubiquitously the enzymatic activity. The loxP recombination triggered the excision of *lano/LRRC1* exon 5 to 7 and of the entire neomycine-resistance cassette.

The (*Lano*^{-/-}) were characterized by PCR and sequencing of the remaining genomic region. Finally, absence of Lano protein expression was tested biochemically on recombinant tissues. Primers used for routine genotyping of mice biopsies are the following: Cre detection

[CreF: TTCCCGCAGAACCTGAAGATGTTCCG; CreR: GGGTGTATAAGCAATCCCCAGAAATGC];

WT gene [LanoWTF: CTTAGTTCAGGGAGTGGTCCG; LanoWT(4R): TTTTCAATCTCCCTGTGGCA];

Floxed Lano/LRRC1 gene [LanoCKO(1F):TTCTGCAGTTGAGAGGCCCATAGT; LanoCKO(5R): AGAACCTGCGTGCAATCCATCTTG]; Lano/LRRC1 excised gene [LanoCKO(1F); LanoWT(4R)].

All experiments were performed in agreement with the French Guidelines for animal handling and approved by local ethics committee APAFIS#10719-2017071709337799. NOD/SCID/ γ c null mice (NSG) were obtained from Charles River (Margate, UK). Mice were housed under sterile conditions with sterilized food and water provided *ad libitum* and maintained on a 12-h light and 12-h dark cycle. 1×10^6 luciferase-expressing SUM149 cells suspended in 50% phenol red-free Matrigel (Becton Dickinson Bioscience) were inoculated in the mammary fat pad in 3 cohorts of 8 mice. Tumor growth was monitored by measuring with a digital caliper and calculating tumor volume ($\text{length} \times \text{width}^2 \times \pi/6$). All animals were randomly assigned to treatment groups, such that the mean tumor volume for each group was 100 to 200 mm³. Bioluminescence analysis was performed using PhotonIMAGER (Biospace Lab) following addition of endotoxin-free luciferin (30 mg/kg). After completion of the analysis, autopsy of mice was performed, and organ luminescence was assessed.

For the limiting dilution assay, 100; 1,000; 100,000 cells were injected as described above in the mammary fat pad of NSG mice corresponding (9 cohorts of 4 mice). Estimation of the breast CSC frequency was calculated using ELDA algorithm.

Supplementary References

El Helou, R., Pinna, G., Cabaud, O., Wicinski, J., Bhajun, R., Guyon, L., Rioualen, C., Finetti, P., Gros, A., Mari, B., et al. (2017). miR-600 Acts as a Bimodal Switch that Regulates Breast Cancer Stem Cell Fate through WNT Signaling. *Cell Rep* 18, 2256-2268.

Finetti, P., Cervera, N., Charafe-Jauffret, E., Chabannon, C., Charpin, C., Chaffanet, M., Jacquemier, J., Viens, P., Birnbaum, D., and Bertucci, F. (2008). Sixteen-kinase gene expression identifies luminal breast cancers with poor prognosis. *Cancer Res* 68, 767-776.

Parker, J.S., Mullins, M., Cheang, M.C., Leung, S., Voduc, D., Vickery, T., Davies, S., Fauron, C., He, X., Hu, Z., et al. (2009). Supervised risk predictor of breast cancer based on intrinsic subtypes. *J Clin Oncol* 27, 1160-1167.

Saito, H., Santoni, M.J., Arsanto, J.P., Jaulin-Bastard, F., Le Bivic, A., Marchetto, S., Audebert, S., Isnardon, D., Adelaide, J., Birnbaum, D., et al. (2001). Lano, a novel LAP protein directly connected to MAGUK proteins in epithelial cells. *J Biol Chem* 276, 32051-32055.

Sebbagh, M., Santoni, M.J., Hall, B., Borg, J.P., and Schwartz, M.A. (2009). Regulation of LKB1/STRAD localization and function by E-cadherin. *Curr Biol* 19, 37-42.